

**A Defective Thesis: Studying the Behaviour of Defects in  
Liquid-Crystalline Materials**

by

**A. A. S. Green**

B.Sc., University of Calgary 2011

M.S., University of Colorado at Boulder 2015

A thesis submitted to the  
Faculty of the Graduate School of the  
University of Colorado in partial fulfillment  
of the requirements for the degree of  
Doctor of Philosophy  
Department of Physics  
2019

This thesis entitled:  
A Defective Thesis: Studying the Behaviour of Defects in Liquid-Crystalline Materials  
written by A. A. S. Green  
has been approved for the Department of Physics

---

Prof. Noel Clark

---

Who knows

---

Please, someone

Date \_\_\_\_\_

The final copy of this thesis has been examined by the signatories, and we find that both the content and the form meet acceptable presentation standards of scholarly work in the above mentioned discipline.

Green, A. A. S. (Ph.D., Physics)

A Defective Thesis: Studying the Behaviour of Defects in Liquid-Crystalline Materials

Thesis directed by Prof. Noel Clark

Often the abstract will be long enough to require more than one page, in which case the macro “\OnePageChapter” should *not* be used.

But this one isn’t, so it should.

## **Dedication**

To all of the fluffy kitties.

## Acknowledgements

Here's where you acknowledge folks who helped. But keep it short, i.e., no more than one page, as required by the Grad School Specifications.

## Contents

### Chapter

<b>1</b>	<b>Introduction</b>	<b>1</b>
1.1	Liquid Crystals . . . . .	1
1.1.1	Phases of matter . . . . .	1
1.1.2	The Rod Liquid Crystal . . . . .	1
1.1.3	The Bent Liquid Crystal . . . . .	1
1.1.4	Characterization of Liquid Crystals: Case Study . . . . .	1
1.2	Fluid Dynamics . . . . .	1
1.3	Fluid Dynamics of Liquid Crystals . . . . .	1
<b>2</b>	<b>The Discovery of Helicity in Tilted Bent-Core Smectics: <math>\text{Sm}(\text{CP})_\alpha</math></b>	<b>2</b>
2.1	A Brief History of Chirality in Bent-Core Smectics . . . . .	2
2.1.1	Conventional Phase of PAL30 . . . . .	2
2.2	Characteristics of the $\text{Sm}(\text{CP})_\alpha$ phase . . . . .	4
2.2.1	The PAL30 Molecule and Phases . . . . .	4
2.2.2	Textures of the $\text{Sm}(\text{CP})_\alpha$ phase . . . . .	4
2.2.3	Electro-Optic Behaviour of the $\text{Sm}(\text{CP})_\alpha$ phase . . . . .	8
2.2.4	Freely-Suspended Films of the $\text{Sm}(\text{CP})_\alpha$ phase . . . . .	10
2.2.5	X-ray Analysis of the $\text{Sm}(\text{CP})_\alpha$ phase . . . . .	10
2.3	Discussion of the $\text{Sm}(\text{CP})_\alpha$ phase . . . . .	13

<b>3 Chirality on Demand: The Discovery of activated Chirality in Achiral Bent-Cores</b>	<b>15</b>
3.1 A history of de Vries phases in liquid crystals . . . . .	15
3.2 Characteristic behaviour of the bent-core de Vries phase . . . . .	15
3.2.1 Textures of bent-code de Vries phase . . . . .	15
3.2.2 Electro-optics of bent-core de Vries phase . . . . .	15
3.2.3 X-ray analysis of bent-core de Vries phase . . . . .	15
3.3 Model for the bent-core de Vries phase . . . . .	15
<b>4 Metrology Applications of Fluid Crystals</b>	<b>18</b>
4.1 . . . . .	18
<b>Bibliography</b>	<b>19</b>

## Appendix

## Tables

### Table

## Figures

### Figure

2.1	.....	3
2.2	.....	3
2.3	Textures of the $\text{Sm}(\text{CP})_\alpha$ phase of PAL30: reminiscent of a $\text{SmC}_\text{A}\text{P}_\text{A}$ texture.	4
2.4	Dynamic optical tilt of $\text{Sm}(\text{CP})_\alpha$ . On application of a field, the state briefly passes through a ‘dark’ state, where the contrast decreases.	6
2.5	Homeotropic textures of PAL30. The relevant temperatures for the Sm2 phases are 104 °C, and 98 °C. The biaxiality in the Sm2 is distinguished by a small ‘hump’ with small applied field, that gets larger on cooling, and changes in character on cooling through the $\text{Sm2} \rightarrow \text{Sm3}$ phase transition at 99 °C, where it broadens. Reproduced from Sreenilayam et al[5].	7
2.6	Series of polarization current measurements taken in the Sm2 phase of PAL30	9
2.7	Polarization current of Sm2 of PAL30 plotted against applied voltage	9
2.8	SAXS of $\text{Sm}(\text{CP})_\alpha$ . The smectic layer size, $d$ , increases monotonically on cooling, with no inflection points that would be characteristic of a untilted $\rightarrow$ tilted phase transition.	10
2.9	Diffractogram of PAL30 taken in the coexistence region between the $\text{Sm}(\text{CP})_\alpha$ ( $q \approx 0.04/\text{\AA}$ ) and the $\text{SmC}_\text{A}\text{P}_\text{A}$ ( $q \approx 0.06/\text{\AA}$ ).	11

2.10 Temperature behaviour of the $\text{Sm}(\text{CP})_\alpha$ phase plotted as a waterfall plot in (a), and as a contour plot in (b). A bilayer ( $d = 112 \text{ \AA} = 2d_0$ ) corresponds to the 2-layer unit-cell structure of the $\text{SmC}_\text{AP}_\text{A}$ phase, which sits directly below the $\text{Sm}(\text{CP})_\alpha$ phase in temperature. The resonant peak corresponding to the $\text{Sm}(\text{CP})_\alpha$ phase at $d \approx 150 \text{ \AA}$ is direct evidence that the $\text{Sm}(\text{CP})_\alpha$ phase is not a classic B2-type phase. . . . .	12
2.11 X-ray scattering from PAL30. (a) SAXS gives a peak from the smectic layer ordering at $q = q_0$ . The RSoXS peak at $q_H$ indicates that there is superlayer orientational ordering with periodicity $d_H$ in the Sm2 phase. In general, superlayer orientational modulation in a smectic generates RSoXS peaks at wavevectors along the layer normal at $q(l, m) = l(2\pi/d_0) \pm m(2\pi/d_H)$ [1]. The observation of an RSoXS reflection at $q = q(0, 1)$ and the absence of an Umklapp peak at $q = q(1, -1)$ in the Sm2 confirms a superlayer helix with a scattering amplitude modulation due to the smectic layering that is undetectably weak. (b) Temperature dependence of resonant scattering. The helix peak at $q_H \approx 1/(2.8d_0)$ becomes diffuse in the Sm3 phase. Splitting of the bilayer peak at $q_B$ , which would indicate helical precession of the bilayer structure, is not observed. . . . .	14
3.1 . . . . .	15
3.2 . . . . .	16
3.3 . . . . .	16
3.4 . . . . .	17
3.5 . . . . .	17

## **Chapter 1**

### **Introduction**

#### **1.1 Liquid Crystals**

**1.1.1 Phases of matter**

**1.1.2 The Rod Liquid Crystal**

**1.1.3 The Bent Liquid Crystal**

**1.1.4 Characterization of Liquid Crystals: Case Study**

#### **1.2 Fluid Dynamics**

#### **1.3 Fluid Dynamics of Liquid Crystals**

## Chapter 2

### The Discovery of Helicity in Tilted Bent-Core Smectics: $\text{Sm}(\text{CP})_\alpha$

The interplay between polarization and chirality has always been front and centre in the development of the banana phases of liquid crystals. From the short-range (bilayer) chiral B2 phases[2], to the long-range helicity of the twist-bend nematic phase, bent-core liquid crystals have been an interesting playground to observe the emergence of spontaneous chirality.

Our discovery of a B2-like phase, with polar, ferrielectric switching that also has a spontaneous twist-bend like helix is the first link between the twist-bend and B2 phases.

#### 2.1 A Brief History of Chirality in Bent-Core Smectics

##### 2.1.1 Conventional Phase of PAL30

To briefly recap Section 1.1.4, the low-temperature phases of PAL30 are conventional B2 phases: the  $\text{SmC}_\text{A}P_\text{A}$  and the  $\text{SmC}_\text{A}P_\text{F}$ . The conventional representation of the polarization current for the Sm3 and Sm4 phases are shown in Figure 2.1.

However, it the switching dynamics of the phases become more clear if the polarization current is plotted directly against the driving voltage, shown in Figure 2.2

This is the end of this section.

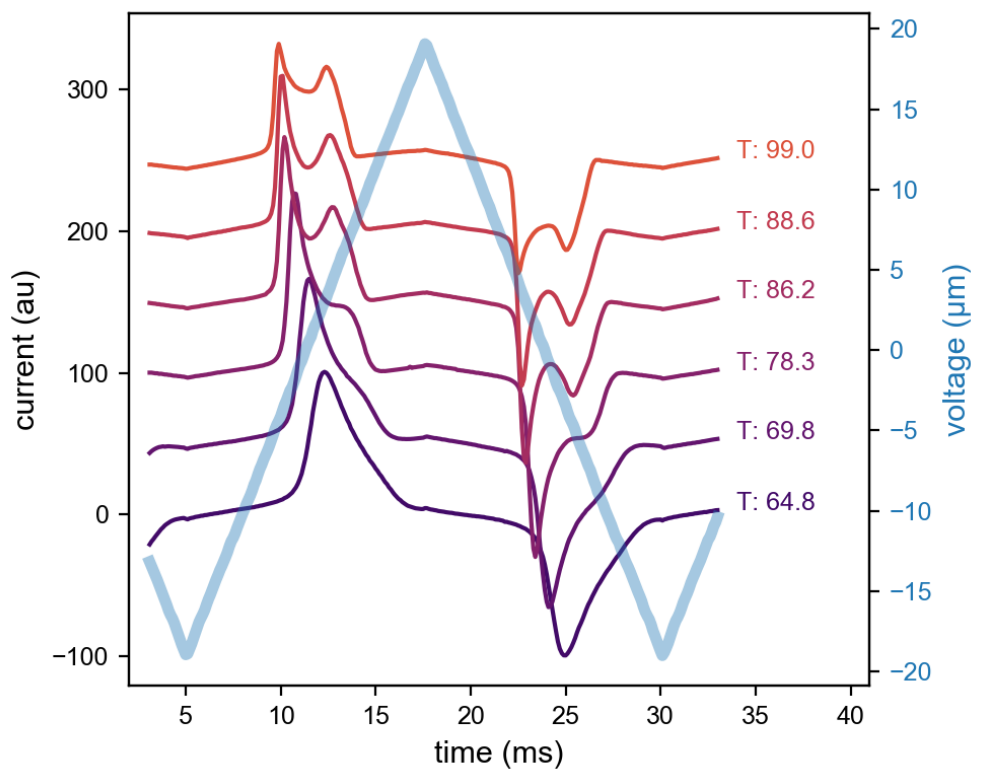


Figure 2.1:

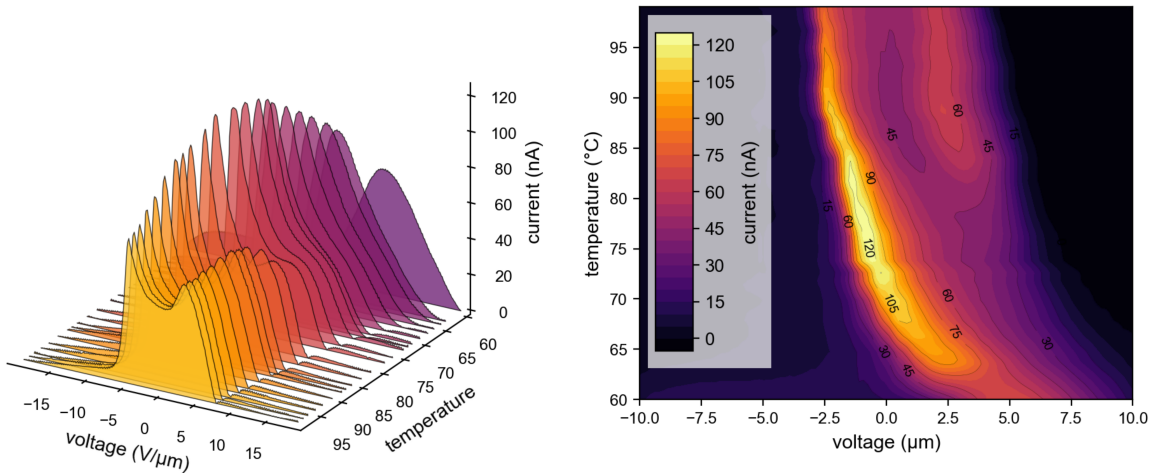


Figure 2.2:

## 2.2 Characteristics of the $\text{Sm}(\text{CP})_\alpha$ phase

### 2.2.1 The PAL30 Molecule and Phases

Go bottom up, to get the boring phases out of the way. (maybe put this in the introduction of PAL30)

add phase description with Sm2

### 2.2.2 Textures of the $\text{Sm}(\text{CP})_\alpha$ phase

#### 2.2.2.1 Planar Aligned Textures

As discussed in Section ??, in planar-aligned cells, the optic axis of the liquid crystal is perpendicular to the  $\vec{k}$  of the applied light—meaning we will be sensitive to relative orientations of the long-axis.

In Figure 2.3, the planar textures of the Sm2 phase of PAL30 are shown. Comparing these with previously published textures reveals a strong similarity to the  $\text{SmC}_\text{A}P_\text{A}$  phases[2, 4]. As discussed in Section ??, the PAL30 phase directly below the Sm2 is a  $\text{SmC}_\text{A}P_\text{A}$ , but with strikingly long-range and regular conglomerate chiral structure, where the handedness is grouped together into stripes. There exists no clear phase transition in the textures between the Sm2 and Sm3 in planar aligned cells.

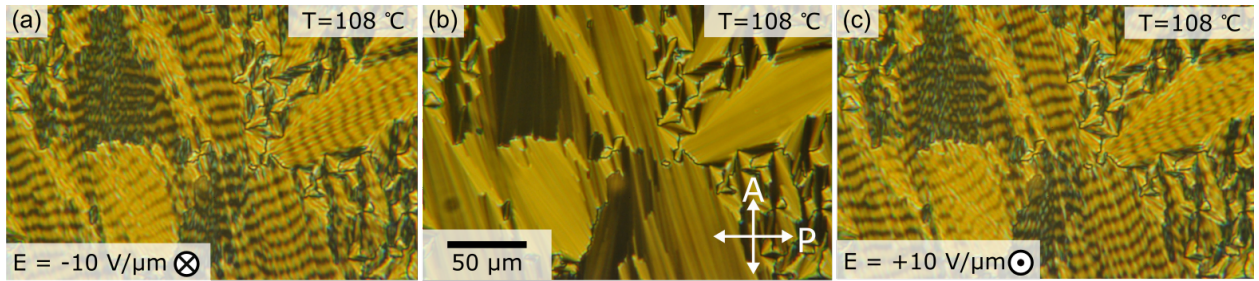


Figure 2.3: Textures of the  $\text{Sm}(\text{CP})_\alpha$  phase of PAL30: reminiscent of a  $\text{SmC}_\text{A}P_\text{A}$  texture.

This similarity is due to the fact that, broadly, the  $\text{SmC}_\text{A}P_\text{A}$  and  $\text{Sm}(\text{CP})_\alpha$  phases are identical optically. Both phases have unit-cells whose dielectric tensor is uniaxial (where the  $\epsilon_{xx} = \epsilon_{yy}$ ), so the optic axis will be parallel to the layer normal and the texture appears like a SmA in it's ground

state.

Both phases are polar, so with a high enough field both states will switch into an aligned SmC<sub>S</sub>P<sub>F</sub> state, which gives a birefringent contrast between domains with different handedness. This contrast is because of the synclinic nature of the SmC<sub>S</sub>P<sub>F</sub> phase—because the tilt is now aligned between the subsequent layers, the phase can organize into conglomerate chiral domains with the optic axis tilted with respect to the layer normal.

We can directly measure the optical tilt in the switched state, by simply rotating the stage when a field has been applied such that an initially dark stripe becomes completely bright. The angle of this rotation is  $2\theta_{opt}$ . To observe the tilt dynamics, we have to extend this analysis as we cannot rotate a stage at the 20 Hz frequency that these samples usually switch at.

We can extract a measurement of the dynamic optical tilt,  $\theta_{opt}$ , by examining the contrast between the bright and dark regions of the stripe. Knowing that the brightness of a birefringent material viewed under cross polarizers is  $I \propto \sin(2\theta)^2$ , the contrast between a “bright” and adjacent “dark” stripe is given by:

$$C = \delta I = I_{\text{bright}} - I_{\text{dark}} = \sin(2\theta_b)^2 - \sin(2\theta_d)^2 \quad (2.1)$$

$$= \frac{1 - \cos(4\theta_b)}{2} - \frac{1 - \cos(4\theta_d)}{2} \quad (2.2)$$

$$= -\sin(2i(\theta_d + \theta_b)) \sin(2(\theta_d - \theta_b)) \quad (2.3)$$

Because of the symmetry of the SmC<sub>S</sub>P<sub>F</sub> state, we know that  $\theta_d = -\theta_b$  (the magnitude of the tilt is equal, but the sign depends on the chirality).

This allows to directly connect the contrast with the tilt angle:

$$C \propto \sin(4\theta_{opt}). \quad (2.4)$$

This analysis assumes that the state we are measuring can be roughly approximated by a SmC<sub>S</sub>P<sub>F</sub>. This will be a good approximation at high field strengths, but may be false at lower fields, where the helix of the Sm(CP) <sub>$\alpha$</sub>  phase may be distorted, but not switched.

Plotting the result in [Figure 2.4](#) we see thresholdless optical switching, where the contrast

figure  
describ-  
ing this  
switching  
mecha-  
nism

(optical tilt) increases linearly with applied field. Interestingly, the  $\text{Sm}(\text{CP})_\alpha$  phase accesses a ‘dark’ state, which was also seen in homeotropic cells, shown in [Figure 2.5](#). This will be discussed in further detail in ??

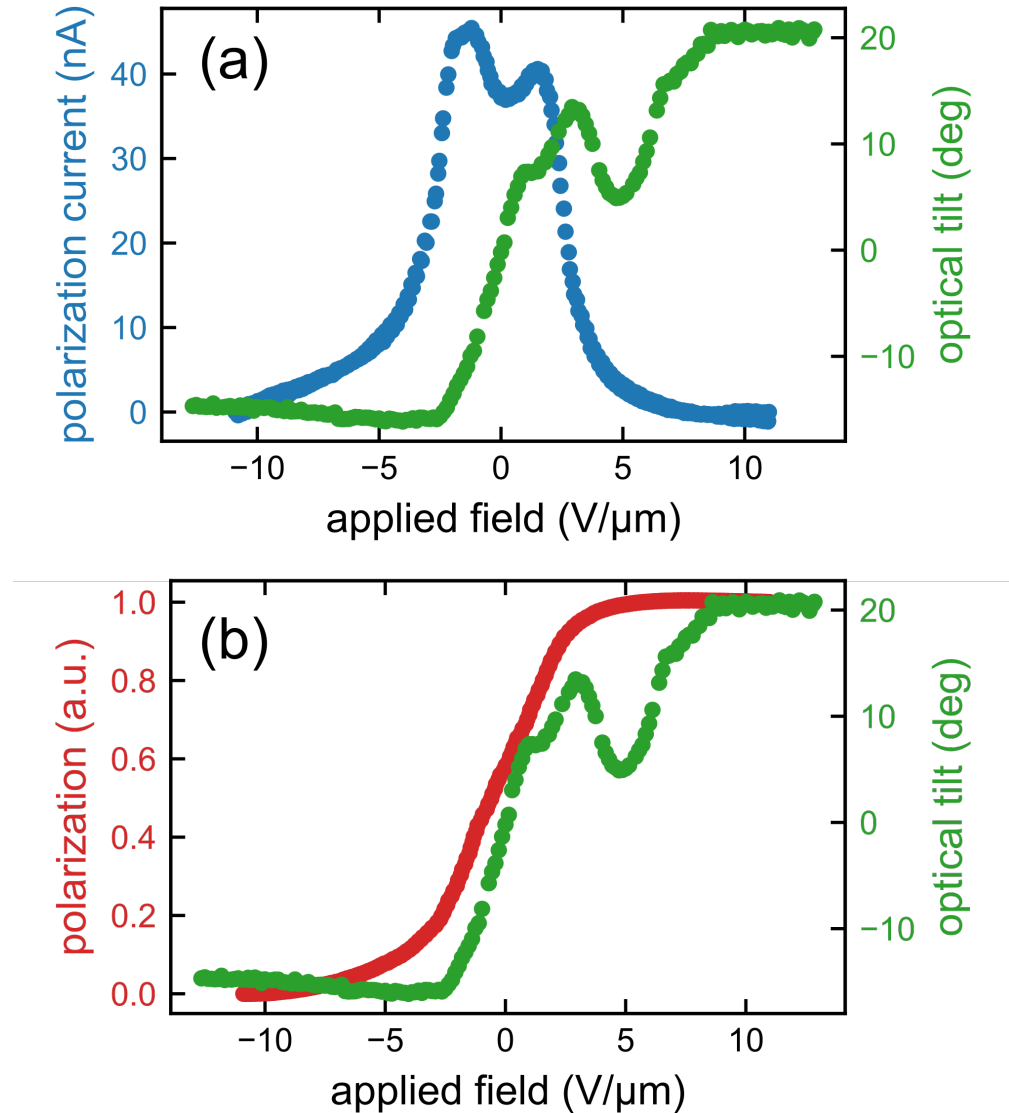


Figure 2.4: Dynamic optical tilt of  $\text{Sm}(\text{CP})_\alpha$ . On application of a field, the state briefly passes through a ‘dark’ state, where the contrast decreases.

In conclusion, the textures of the  $\text{Sm}(\text{CP})_\alpha$  phase have identical characteristics to those of the  $\text{SmC}_\text{A} \text{PA}$ , though an interesting dark state emerges when viewed under dynamic conditions.

### 2.2.2.2 Homeotropic Aligned Textures

Though we were unable to achieve good homeotropic alignment, we can rely on the published results of the Dublin group, who published a series of papers on the PAL30 homolog series[3, 5, 6, 7]. Though their interpretation is wrong (PAL30 is not an orthogonal phase), they report beautifully aligned homeotropic textures and study the response of these textures to an applied in-plane electric field. These textures are reproduced from Sreenilayam et al[5] in [Figure 2.5](#).

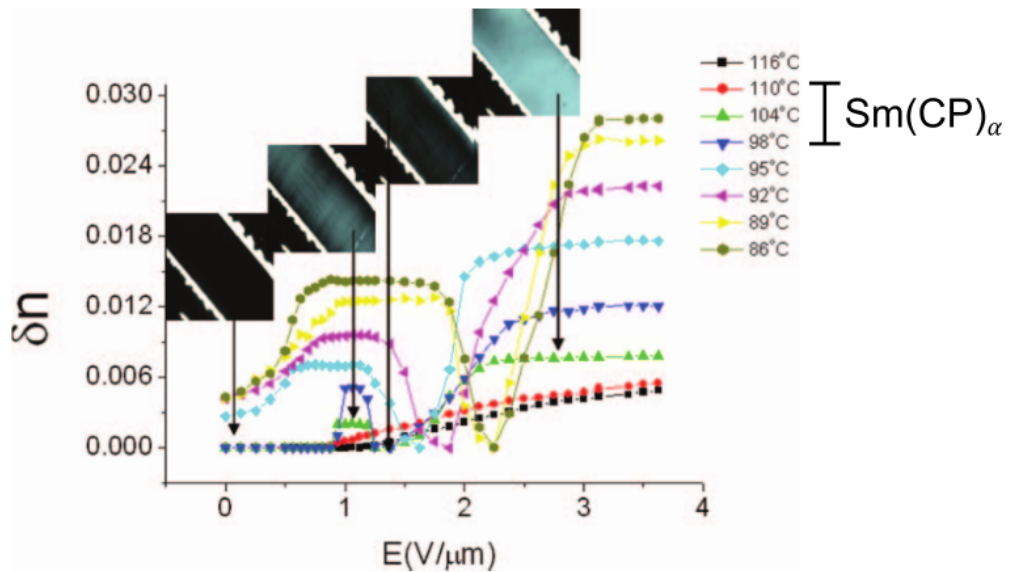


Figure 2.5: Homeotropic textures of PAL30. The relevant temperatures for the Sm2 phases are 104 °C, and 98 °C. The biaxiality in the Sm2 is distinguished by a small ‘hump’ with small applied field, that gets larger on cooling, and changes in character on cooling through the Sm2→Sm3 phase transition at 99 °C, where it broadens. Reproduced from Sreenilayam et al[5].

The phase of interest,  $\text{Sm}(\text{CP})_\alpha$  occurs in the temperature range 110 °C to 99 °C. There is a clear change in the field-behaviour of the biaxiality at the Sm2→Sm3 transition temperature. However, because these phases are tilted the authors original interpretation of the data needs to be revisited.

For our purposes, we can use these textures to distinguish the  $\text{Sm}(\text{CP})_\alpha$  phase from the closely related  $\text{SmCP}_\text{A}$  phase. The  $\text{SmCP}_\text{A}$  phase should be weakly biaxial in homeotropic cells. The anticlinic structure should ‘average’ out any anisotropy in the dielectric tensor due to the tilt of the

molecule, but because these are bent-core phases, there is a built in anisotropy of the dielectric tensor due to the rotation symmetry breaking of the banana structure, which should manifest in homeotropic cells as a schlieren texture that allows for  $\pm 1/2$  defects.

From [Figure 2.5](#), it is clear that, for the temperature ranges of  $\text{Sm}(\text{CP})_\alpha$  the textures appear dark— they have no measurable biaxiality. This means that the inherent anisotropy of the dielectric tensor of the molecule *must* be organized in a structure that averages it out. This is a clue to the helical nature of the  $\text{Sm}(\text{CP})_\alpha$ .

### **2.2.3      Electro-Optic Behaviour of the $\text{Sm}(\text{CP})_\alpha$ phase**

We can study the electro-optic behaviour of PAL30 in both homeotropic and planar aligned cells. In homeotropic, you are studying the *biaxiality* of the phase, ie. the birefringence  $\delta n = n_2 - n_3$ . In planar aligned cells, you are studying the birefringence between the molecules long axis and some weighted combination of  $n_2$  and  $n_3$  that depends on the orientation.

There are two categories of behaviour you can track to get information about the phase: the polarization current and the birefringence/biaxiality.

#### **2.2.3.1    Polarization Current**

The  $\text{Sm}(\text{CP})_\alpha$  phase manifests a slight ferrielectric behaviour, where three peaks are visible under a high resolution polarization current trace. Broadly, the phase appears to have two main peaks, usually associated with antiferroelectric behaviour.

However, the differences between these two phases becomes apparent under the application of an electric field. This is because the sequence of intermediate phases between a  $\text{SmC}_\text{A}P_\text{A} \rightarrow \text{SmC}_\text{S}P_\text{F}$  is different from  $\text{Sm}(\text{CP})_\alpha \rightarrow \text{SmC}_\text{S}P_\text{F}$ . If the bent-core  $\text{Sm}(\text{CP})_\alpha$  phase behaves like its calamitic cousin, the  $\text{SmC}^*_\alpha$ , then under application of a field perpendicular to the helical axis, the helix of the  $\text{Sm}(\text{CP})_\alpha$  distorts. This helical distortion is likely causing the three peaks visible in [Figure 2.7](#).

A more conventional series of traces for the polarization current is shown in [Figure 2.6](#), where the current is plotted as a function of time. The same data is shown in [Figure 2.7](#), where the current

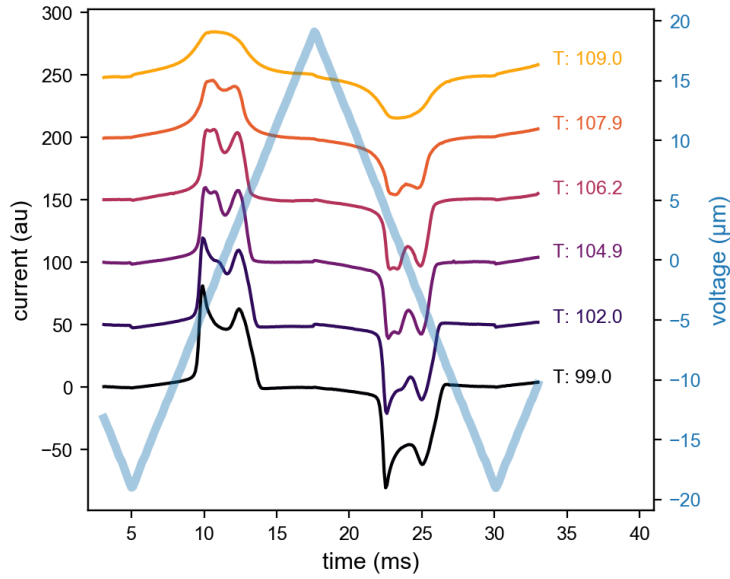


Figure 2.6: Series of polarization current measurements taken in the Sm2 phase of PAL30

is plotted directly against the applied voltage.

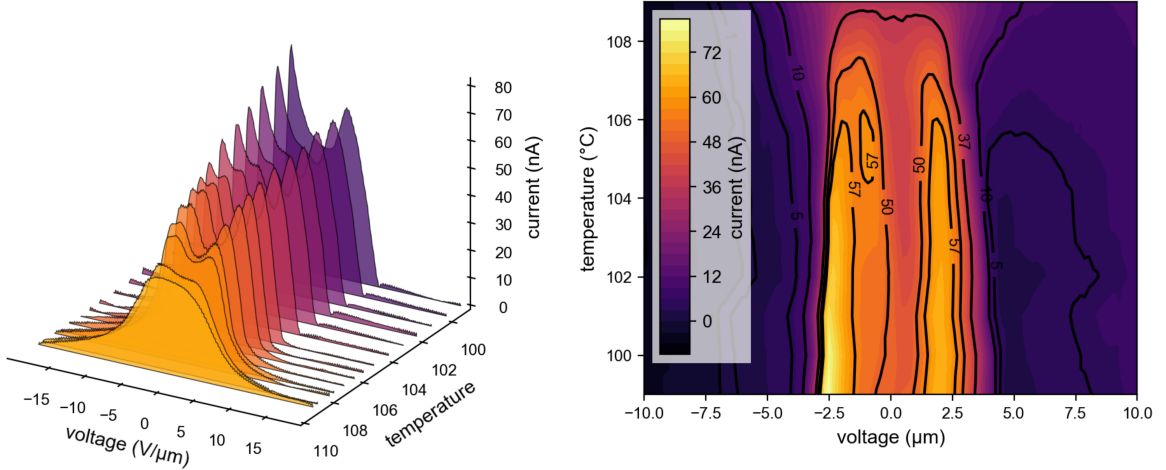


Figure 2.7: Polarization current of Sm2 of PAL30 plotted against applied voltage

A more conventional series of traces for the polarization current is shown in [Figure 2.6](#), where the current is plotted as a function of time. The same data is shown in [Figure 2.7](#), where the current is plotted directly against the applied voltage. The

#### 2.2.4 Freely-Suspended Films of the $\text{Sm}(\text{CP})_\alpha$ phase

#### 2.2.5 X-ray Analysis of the $\text{Sm}(\text{CP})_\alpha$ phase

The two techniques used to characterize the  $\text{Sm}(\text{CP})_\alpha$  phase were SAXS (small angle hard x-ray scattering) and RSoXS (resonant soft x-ray scattering). As the SAXS is sensitive to periodicity in electron density, we can directly measure the smectic layer size ( $d$ ), as shown in [Figure 2.8](#).

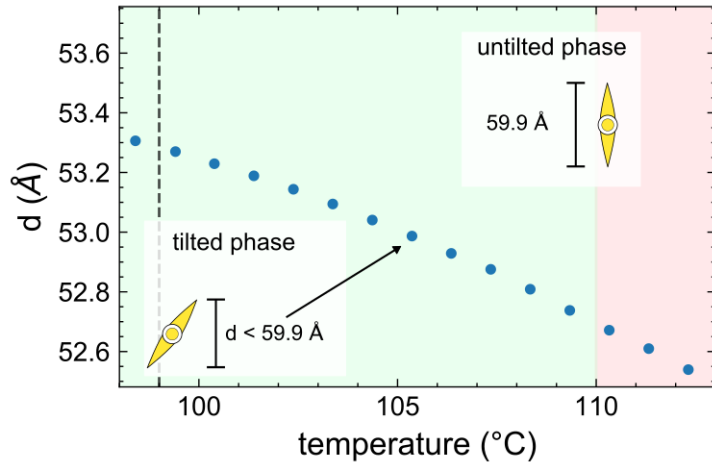


Figure 2.8: SAXS of  $\text{Sm}(\text{CP})_\alpha$ . The smectic layer size,  $d$ , increases monotonically on cooling, with no inflection points that would be characteristic of a untilted  $\rightarrow$  tilted phase transition.

The smectic layer size is measurably smaller than the length of an extended molecule, which supports the classification of  $\text{Sm}(\text{CP})_\alpha$  as a tilted phase. However, the increase seen on cooling, which stands in contrast to the majority of bent-core materials, may indicate a significant amount of intercalation at higher temperatures.

The x-ray analysis can be greatly supplemented with the addition of resonant scattering, which is sensitive to periodicity in orientation. A resonant diffractogram taken at  $104^\circ\text{C}$  is shown in [Figure 2.9](#).

By azimuthally averaging diffractograms like the one in [Figure 2.9](#) and plotting them as a function of temperature, [Figure 2.10](#), the behaviour of the  $\text{Sm}(\text{CP})_\alpha$  phase can be determined over its entire temperature range.

The resonant peak corresponding to the  $\text{Sm}(\text{CP})_\alpha$  phase ( $d \approx 150 \text{ \AA}$ ) shows that this phase

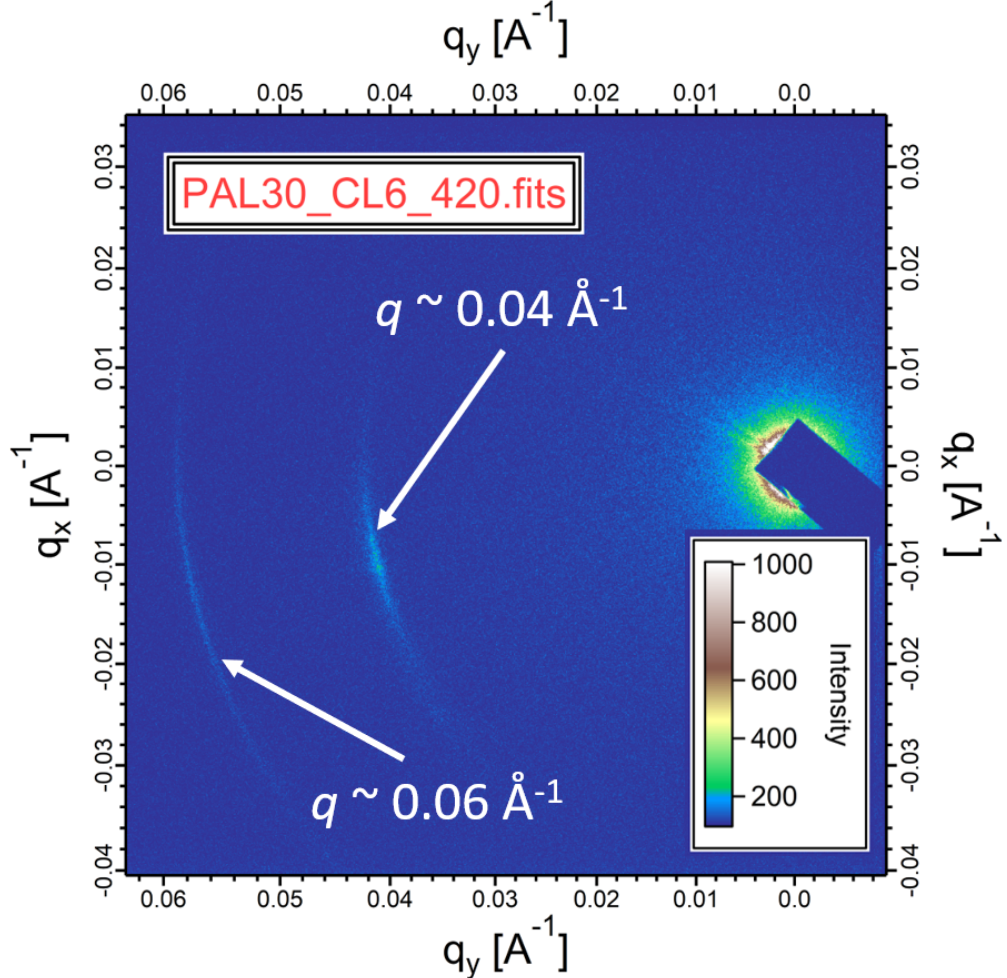


Figure 2.9: Diffractogram of PAL30 taken in the coexistence region between the  $\text{Sm}(\text{CP})_\alpha$  ( $q \approx 0.04/\text{\AA}$ ) and the  $\text{SmCPA}$  ( $q \approx 0.06/\text{\AA}$ ).

cannot be a B2 phase (as those only have one or two layer unit-cells. However, the fact that this feature appears at roughly three times the smectic layer spacing is neccesary but not sufficient for a helix. An example of this type of structure would be the proposed devil-staircase model put forth to explain a similiar phase in phase family of calimitics.

Though a detailed examination of the unit-cell structure of the  $\text{Sm}(\text{CP})_\alpha$  will have to wait on the advent of polarization-resolved resonant x-ray on the carbon K-edge, we can actually confirm the helical nature of the  $\text{Sm}(\text{CP})_\alpha$  phase through careful analysis.

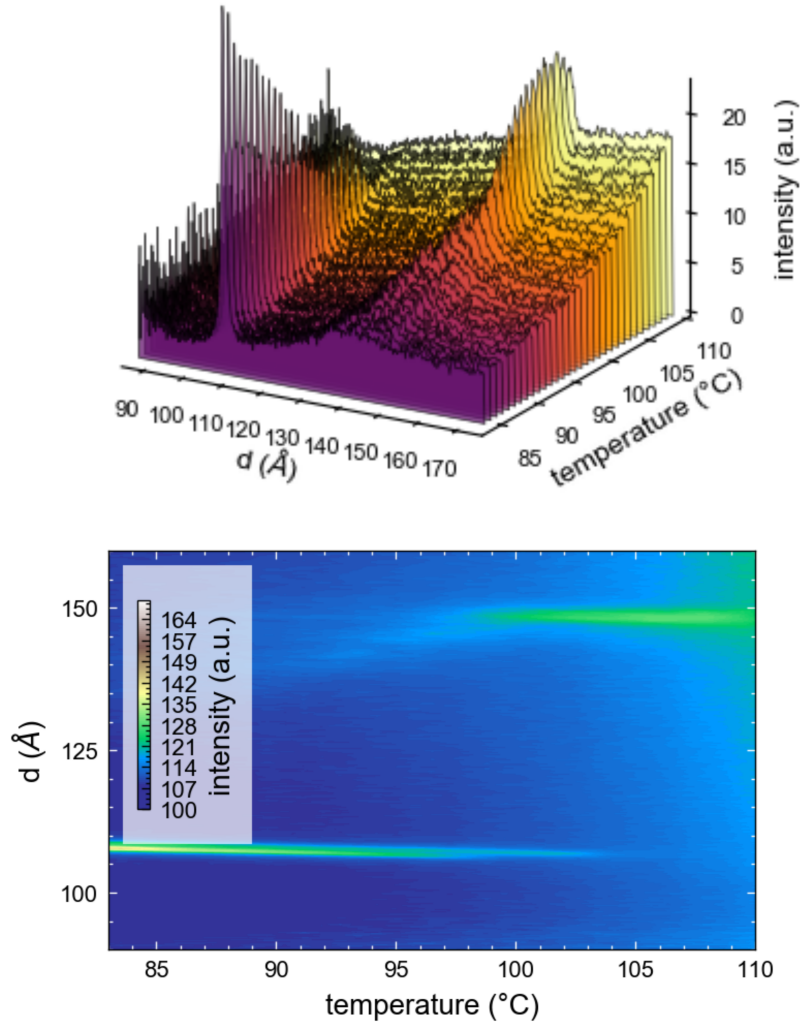


Figure 2.10: Temperature behaviour of the  $\text{Sm}(\text{CP})_{\alpha}$  phase plotted as a waterfall plot in (a), and as a contour plot in (b). A bilayer ( $d = 112 \text{ \AA} = 2d_0$ ) corresponds to the 2-layer unit-cell structure of the  $\text{SmCPA}$  phase, which sits directly below the  $\text{Sm}(\text{CP})_{\alpha}$  phase in temperature. The resonant peak corresponding to the  $\text{Sm}(\text{CP})_{\alpha}$  phase at  $d \approx 150 \text{ \AA}$  is direct evidence that the  $\text{Sm}(\text{CP})_{\alpha}$  phase is not a classic B2-type phase.

### 2.2.5.1 Umklapp Peaks

Though a detailed examination of the unit-cell structure of the  $\text{Sm}(\text{CP})_{\alpha}$  will have to wait on the advent of polarization-resolved resonant x-ray on the carbon K-edge, we can actually confirm the helical nature of the  $\text{Sm}(\text{CP})_{\alpha}$  phase through careful analysis. By combining the SAXS data

and the RSoXS data, we can deduce two things. First, that the resonant feature of the  $\text{Sm}(\text{CP})_\alpha$  phase is incommensurate with the underlying smectic layer spacing. Specifically, it has a unit cell thickness of  $148 \text{ \AA} \approx 2.8d_0$ . Second, that we are missing an expected umklapp (harmonic) peak.

Umklapp is a german word meaning flip-over, and it refers to higher harmonics that are wrapped back into the Brioullon zone. Following Levulet and Pansu [1], where the smectic layers are modeled as stacked tensorial slabs, the master equation that predicts these flip-over harmonics is given by:

$$\frac{q}{q_0} = 2\pi l + 2\pi m \frac{1}{p}, \quad \forall l \in \mathbb{N}, \quad \forall m \in \mathbb{Z} \quad (2.5)$$

where  $q$  is the location of the expected harmonic,  $q_0$  is the scattering off the smectic layer spacing,  $p$  is the pitch (in units of the smectic layer spacing) of the unit-cell,  $l$  is a positive integer, and  $m$  is a positive or negative integer.

From Equation 2.5, we can see one of the nearest harmonics should occur at  $l = 1, m = -1$ . For the  $\text{Sm}(\text{CP})_\alpha$  phase, with a pitch of  $p = 1/2.8$ , we would expect to see a harmonic at  $\frac{1}{2.8}$ . To highlight this analysis, we plot the azimuthally-averaged diffractogram in the co-existence region between the  $\text{Sm}(\text{CP})_\alpha$  and the  $\text{SmC}_\text{A}\text{P}_\text{A}$ , on a  $q$ -scale normalized by the scattering from the smectic layer spacing,  $q_0$ , in Figure 2.11.

include  
this num-  
ber

### 2.3 Discussion of the $\text{Sm}(\text{CP})_\alpha$ phase

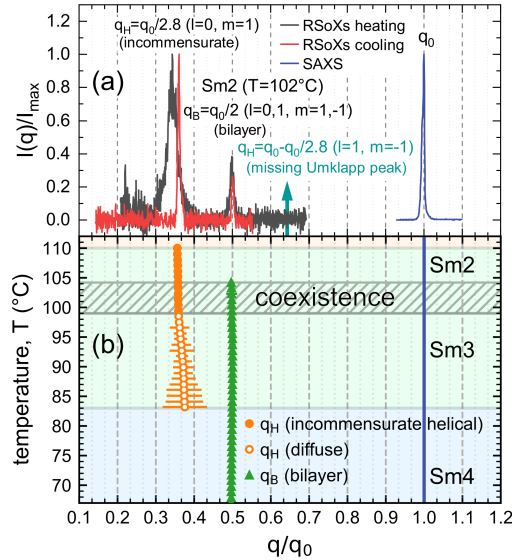


Figure 2.11: X-ray scattering from PAL30. (a) SAXS gives a peak from the smectic layer ordering at  $q = q_0$ . The RSoXS peak at  $q_H$  indicates that there is superlayer orientational ordering with periodicity  $d_H$  in the Sm2 phase. In general, superlayer orientational modulation in a smectic generates RSoXS peaks at wavevectors along the layer normal at  $q(l, m) = l(2\pi/d_0) \pm m(2\pi/d_H)$ [1]. The observation of an RSoXS reflection at  $q = q(0, 1)$  and the absence of an Umklapp peak at  $q = q(1, -1)$  in the Sm2 confirms a superlayer helix with a scattering amplitude modulation due to the smectic layering that is undetectably weak. (b) Temperature dependence of resonant scattering. The helix peak at  $q_H \approx 1/(2.8d_0)$  becomes diffuse in the Sm3 phase. Splitting of the bilayer peak at  $q_B$ , which would indicate helical precession of the bilayer structure, is not observed.

## Chapter 3

### Chirality on Demand: The Discovery of activated Chirality in Achiral Bent-Cores

#### 3.1 A history of de Vries phases in liquid crystals

#### 3.2 Characteristic behaviour of the bent-core de Vries phase

##### 3.2.1 Textures of bent-core de Vries phase

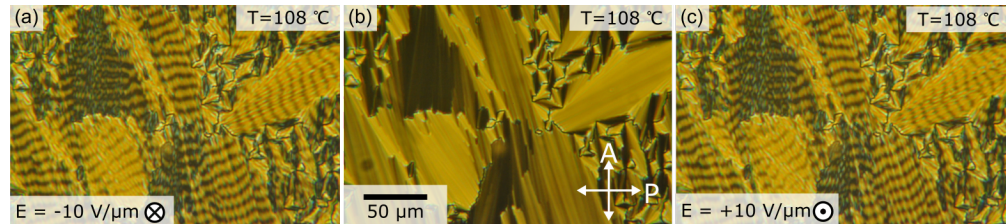


Figure 3.1:

##### 3.2.2 Electro-optics of bent-core de Vries phase

text text

text

##### 3.2.3 X-ray analysis of bent-core de Vries phase

#### 3.3 Discussion for the bent-core de Vries phase

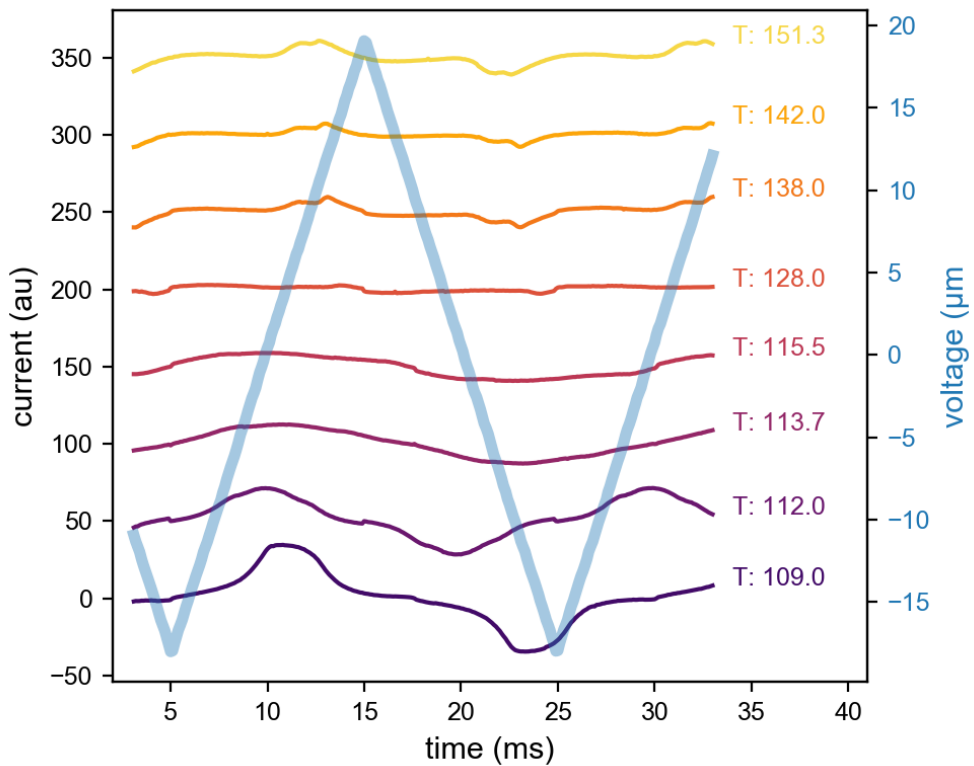


Figure 3.2:

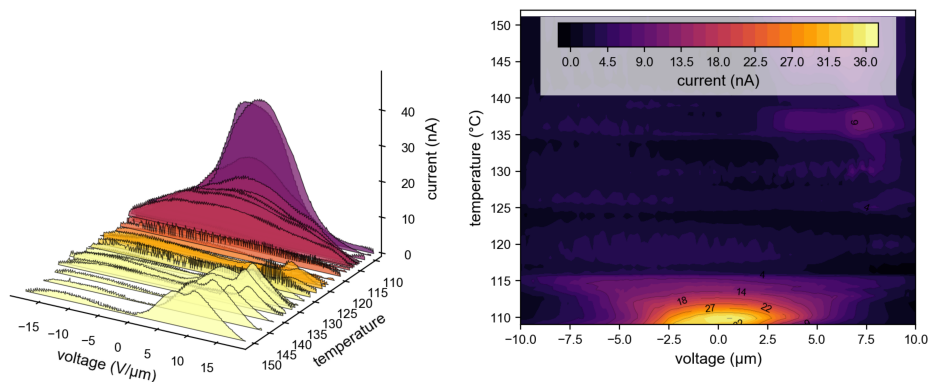


Figure 3.3:

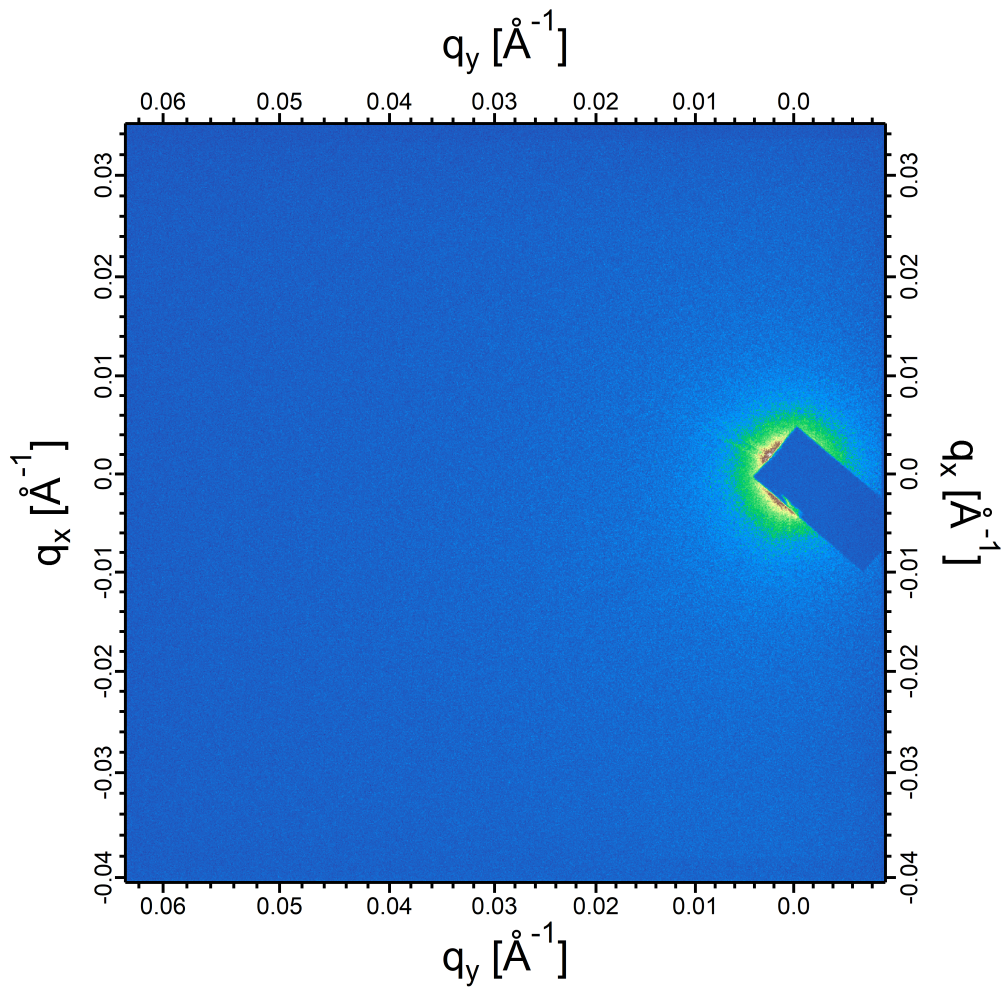


Figure 3.4:

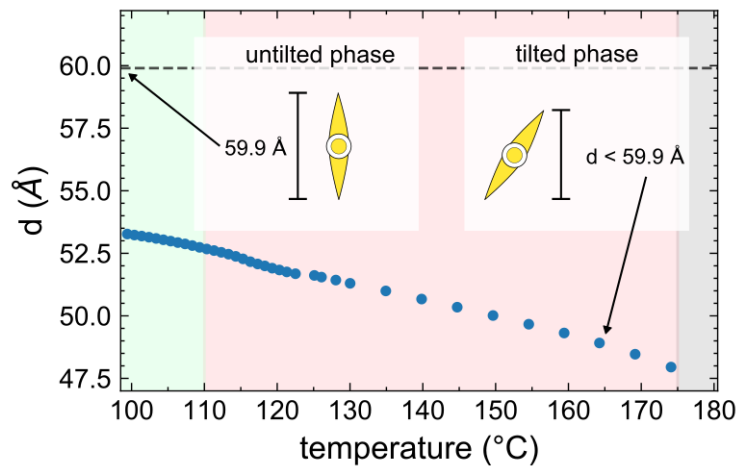


Figure 3.5:

## **Chapter 4**

### **Metrology Applications of Fluid Crystals**

**4.1**

## Bibliography

- [1] Anne-Marie Levelut and Brigitte Pansu. Tensorial x-ray structure factor in smectic liquid crystals. Phys. Rev. E, 60(6):6803, 1999.
- [2] Darren R. Link, Giorgio Natale, Renfan Shao, Joseph E. MacLennan, Noel A. Clark, Eva Körblova, and David M. Walba. Spontaneous Formation of Macroscopic Chiral Domains in a Fluid Smectic Phase of Achiral Molecules. Science, 278(5345):1924–1927, December 1997.
- [3] Y. P. Panarin, M. Nagaraj, S. Sreenilayam, J. K. Vij, A. Lehmann, and C. Tschierske. Sequence of four orthogonal smectic phases in an achiral bent-core liquid crystal: Evidence for the  $\text{smap}_\alpha$  phase. Phys. Rev. Lett., 107(24):247801, December 2011.
- [4] R. Amaranatha Reddy and B. K. Sadashivaa. Influence of fluorine substituent on the mesomorphic properties of five-ring ester banana-shaped molecules. 30(9):1031–1050.
- [5] S. Sreenilayam, M. Nagaraj, Y. P. Panarin, J. K. Vij, A. Lehmann, and C. Tschierske. Properties of Non-Tilted Bent-Core Orthogonal Smectic Liquid Crystal. Mol. Cryst. Liq. Cryst., 553(1):140–146, January 2012.
- [6] S. Sreenilayam, Yu. P. Panarin, J. K. Vij, A. Lehmann, and C. Tschierske. Occurrence of Five Different Orthogonal Smectic Phases in a Bent-Core (BC) Liquid Crystal. 610(1):116–121.
- [7] Sithara P. Sreenilayam, Yuri P. Panarin, Jagdish K. Vij, Vitaly P. Panov, Anne Lehmann, Marco Poppe, Marko Prehm, and Carsten Tschierske. Spontaneous helix formation in non-chiral bent-core liq. cryst. with fast linear electro-optic effect. Nat. Commun., 7:11369, May 2016.